Biophysical Journal
Article

Biophysical Society

The Water Permeability and Pore Entrance Structure of Aquaporin-4 Depend on Lipid Bilayer Thickness

Jihong Tong,[1] Zhe Wu,[2] Margaret M. Briggs,[1] Klaus Schulten,[2,*] and Thomas J. McIntosh[1,*]
[1]Department of Cell Biology, Duke University Medical Center, Durham, North Carolina; and [2]Center for the Physics of Living Cells and Beckman Institute, University of Illinois Urbana-Champaign, Urbana, Illinois

ABSTRACT Aquaporin-4 (AQP4), the primary water channel in glial cells of the mammalian brain, plays a critical role in water transport in the central nervous system. Previous experiments have shown that the water permeability of AQP4 depends on the cholesterol content in the lipid bilayer, but it was not clear whether changes in permeability were due to direct cholesterol-AQP4 interactions or to indirect effects caused by cholesterol-induced changes in bilayer elasticity or bilayer thickness. To determine the effects resulting only from bilayer thickness, here we use a combination of experiments and simulations to analyze AQP4 in cholesterol-free phospholipid bilayers with similar elastic properties but different hydrocarbon core thicknesses previously determined by x-ray diffraction. The channel (unit) water permeabilities of AQP4 measured by osmotic-gradient experiments were $3.5 \pm 0.2 \times 10^{-13}$ cm^3/s (mean ± SE), $3.0 \pm 0.3 \times 10^{-13}$ cm^3/s, $2.5 \pm 0.2 \times 10^{-13}$ cm^3/s, and $0.9 \pm 0.1 \times 10^{-13}$ cm^3/s in bilayers containing (C22:1)(C22:1)PC, (C20:1)(C20:1)PC, (C16:0)(C18:1)PC, and (C13:0)(C13:0)PC, respectively. Channel permeabilities obtained by molecular dynamics (MD) simulations were $3.3 \pm 0.1 \times 10^{-13}$ cm^3/s and $2.5 \pm 0.1 \times 10^{-13}$ cm^3/s in (C22:1)(C22:1)PC and (C14:0)(C14:0)PC bilayers, respectively. Both the osmotic-gradient and MD-simulation results indicated that AQP4 channel permeability decreased with decreasing bilayer hydrocarbon thickness. The MD simulations also suggested structural modifications in AQP4 in response to changes in bilayer thickness. Although the simulations showed no appreciable changes to the radius of the pore located in the hydrocarbon region of the bilayers, the simulations indicated that there were changes in both pore length and α-helix organization near the cytoplasmic vestibule of the channel. These structural changes, caused by mismatch between the hydrophobic length of AQP4 and the bilayer hydrocarbon thickness, could explain the observed differences in water permeability with changes in bilayer thickness.

INTRODUCTION

Aquaporins (AQPs) are water channels located in the plasma membranes of many cells. AQPs are essential for body water homeostasis and cell volume control (1,2), and members of the aquaporin family are implicated in numerous physiological processes as well as a wide range of clinical disorders (3–5). In particular, AQP4 is the primary water channel in the brain that is found in large concentrations in astrocytes along the blood-brain barrier. AQP4 plays a critical role in normal brain function (6–15) and has been implicated in several pathological conditions, including edema (9,12,16–18).

The functional properties of several classes of membrane channels can be modified by the membrane bilayer (19–26). Lundbaek et al. (27) note that there can be a protein-lipid coupling so that "the bilayer becomes an allosteric modulator of membrane protein function." Determination of the effects of bilayer composition on specific membrane proteins is motivated by the differences in membrane lipids observed in different cells, organelles, and membrane microdomains (21–26).

It has recently been shown that the unit water permeabilities of both AQP0 and AQP4 strongly depend on bilayer composition, decreasing with increasing cholesterol concentration (26,28). In addition to specific protein-cholesterol interactions, observed in the case of AQP0 in cholesterol-enriched bilayers (29), cholesterol has two effects on bilayer properties that could potentially modify AQP water permeability. First, cholesterol modifies the elasticity of the bilayer (as measured by the bilayer elastic stress or compressibility modulus), which could potentially restrict the conformational flexibility of the channel pore. Second, cholesterol increases bilayer hydrocarbon thickness (30,31), thereby leading to hydrophobic mismatch between the hydrophobic length of AQP0 or AQP4 and the bilayer hydrocarbon

Submitted April 21, 2016, and accepted for publication May 13, 2016.
*Correspondence: kschulte@ks.uiuc.edu or thomas.mcintosh@duke.edu
Jihong Tong and Zhe Wu contributed equally to this work.
Editor: Andreas Engel.
http://dx.doi.org/10.1016/j.bpj.2016.05.039

thickness, which could potentially modify protein conformation and function. For example, bilayer thickness has been shown to modify the properties of several membrane channels, including gramicidin channels (32–35), KcsA potassium channels (36,37), and BKCa calcium channels (38).

In this article, we further investigate the effects of the lipid bilayer on AQP4 function. Using osmotic-gradient experiments, we measure AQP4 unit permeability in single-component phospholipid bilayers with a wide range of hydrocarbon chain lengths but with similar compressibility moduli (39). We also present molecular dynamics (MD) simulations suggesting AQP4 conformation changes that could potentially lead to different water-conducting rates in phospholipid bilayers with different hydrocarbon chain lengths. The simulation results indicated that decreasing the bilayer hydrocarbon chain length 1) modified the pore-entrance structure in proximity to the bulk reservoir, and 2) increased the total length of the AQP4 pore. Either, or a combination of both, of these structural changes could result in our observed differences in water permeability. In terms of observation 1, the magnitude of the decreased permeability is consistent with a recent theoretical treatment concerning entrance effects and the hourglass shape of aquaporins (40). For observation 2, the increased length of the single-file region of the pore would be expected to increase resistance to water flow.

MATERIAL AND METHODS

Osmotic-gradient water permeability measurements

Expression and purification of AQP4 isoforms

The M23 isoform of aquaporin 4 was expressed and purified by methods detailed by Tong et al. (28). In brief, the plasmid pYES10-His-AQP4-M23 was expressed in the protease-deficient *Saccharomyces cerevisiae* (*pep*4) yeast, and purified as described in Yukutake et al. (41) with some modification. All buffers were supplemented with an EDTA-free protease inhibitor cocktail (Roche, Indianapolis, IN). After ultracentrifugation, the membrane pellet was solubilized in buffer A, which contained 100 mM K_2HPO_4, 10% glycerol, 200 mM NaCl, 5 mM 2-mercaptoethanol, and 2% *n*-octyl-D-glucopyranoside (OG) (Affymetrix, Cleveland, OH). After removing insoluble material by ultracentrifugation, the solubilized proteins were adjusted to 20 mM imidazole and gently mixed overnight with Ni-NTA agarose beads. The beads were washed in a column with 50 mM imidazole in buffer A, and bound AQP4 was eluted with 750 mM imidazole in buffer A. The protein concentration was measured with the bicinchonic acid (BCA) assay using a bovine serum albumin (BSA) standard (Thermo Scientific, Rockford, IL). The absolute accuracy of such protein assays depends on the suitability of the standard protein (BSA). Therefore, for some samples, we also calculated AQP4 concentration by measuring the absorbance at 280 nm (A_{280}) and using the extinction coefficient (43430 M^{-1} cm^{-1}) (http://web.expasy.org/protparam/). Since the A_{280} results were in close agreement with those of the BCA assays (data not shown), we routinely used the BCA assay with the BSA standard. The purity of AQP4 was determined by sodium dodecyl sulfate polyacrylamide gel electrophoresis (SDS-PAGE) and Western blot using antibodies from Santa Cruz Biotechnology (Santa Cruz, California). For SDS-PAGE, protein samples were mixed (1:1) with Laemmli sample buffer containing 10% SDS and analyzed with a 4–20% gel. Gels, stained with Sypro Ruby, imaged and analyzed with a BioChemi System with LabWorks 4.0 (UVP BioImaging System, Upland, CA), showed that the AQP4 was >90% pure.

Reconstitution of AQP4 into proteoliposomes

The phospholipids dierucoylphosphatidylcholine ((C22:1)(C22:1)PC), dieicosenoylphosphatidylcholine ((C20:1)(C20:1)PC), palmitoyloleoylphosphatidylcholine ((C16:0)(C18:1)PC), ditridecanoylphosphatidylcholine ((C13:0)(C13:0)PC), dielaidoylphosphatidylglycerol ((C18:1)(C18:1)PG), and dimyristoylphosphatidylglycerol ((C14:0)(C14:0)PG) were purchased from Avanti Polar Lipids (Alabaster, AL). To obtain bilayers with a range of thicknesses, we used four specific lipid systems: (C22:1)(C22:1)PC/(C18:1)(C18:1)PG, (C20:1)(C20:1)PC/(C18:1)(C18:1)PG, (C16:0)(C18:1)PC/(C18:1)(C18:1)PG, and (C13:0)(C13:0)PC/(C14:0)(C14:0)PG, each with an 8:2 molar ratio of PC to PG. Bilayers formed from each of these PCs have very similar area compressibility moduli, a measure of bilayer elasticity (39). The negatively charged PGs, with hydrocarbon chain compositions similar to the accompanying choline-containing phospholipids, were included to help stabilize large unilamellar proteoliposomes and minimize aggregation. For simplicity, throughout the remainder of this article, we refer to each lipid system by its PC component. An implicit assumption was that the introduction of 20 mol % PG did not appreciably modify the structure of the PC bilayers. Although there are few structural data for liquid-crystalline PG bilayers, neutron and x-ray scattering experiments show that pure (C16:0)(C18:1)PG bilayers have an area per molecule (A_m) of 0.66 ± 0.01 nm^2 and a hydrocarbon thickness (d_{hc}) of 2.79 ± 0.6 nm (42), similar to values of $A_m = 0.68$ nm^2 and $d_{hc} = 2.71$ nm measured for pure (C16:0)(C18:1)PC bilayers (43).

The lipids were mixed in chloroform/methanol, dried by rotary evaporation, and hydrated at 20°C in 25 mM HEPES, 50 mM NaCl, and 2% OG, pH 7.4. The lipids and proteins in OG were mixed at appropriate lipid/protein molar ratios, OG was removed by dialysis for 2 days at 20°C against 25 mM HEPES, 50 mM NaCl, 2 mM dithiothreitol (DTT), and 1 mM PMSF, pH 7.4. The resulting lipid/protein vesicles were collected by ultracentrifugation (26,44) and resuspended in dialysis buffer plus 50 mM sucrose. Large unilamellar proteoliposomes were obtained by extrusion through 100 nm pore filters (Avanti Polar Lipids, Alabaster, AL). For each sample, the average liposome and proteoliposome diameters were determined by quasielastic light scattering with a ZetaPlus Zeta Potential Analyzer (Brookhaven Instruments, Holtsville, NY). Average measured diameters were 134.0 ± 4.7 nm for (C22:1)(C22:1)PC, 131.3 ± 3.7 nm for (C20:1)(C20:1)PC, 116.6 ± 4.7 nm for (C16:0)(C18:1)PC, and 130.1 ± 2.6 nm for (C13:0)(C13:0)PC. For each lipid system, the AQP4 unit water permeabilities were independent of vesicle diameter (data not shown).

The lipid and protein compositions of the proteoliposomes were determined by phosphate assays (45) and SDS-PAGE, respectively. AQP4 in proteoliposomes and known amounts of AQP4 in OG (standardized by BCA assay) were analyzed on the same SDS gel. Integrated optical densities were measured, and the AQP4 concentrations in proteoliposomes were calculated by comparison with the standards, which showed a linear response. This approach was necessary because the bilayer lipids interfered with direct BCA assays.

Measurements of AQP4-proteoliposome water permeability

Water permeabilities were measured using techniques that apply an osmotic gradient with sucrose solutions and determine as a function of time the change in proteoliposome volume due to water efflux (1,3,40,46–51). We measured the volume change at ambient temperature by light scattering with a wavelength of 600 nm (51,52) using an SX20 stopped-flow spectrometer (Applied Photophysics, Leatherhead, UK). The proteoliposome or liposome permeability (p_f), in units of cm/s, was calculated from the formula

$$p_f = k/\{(SAV)(V_W)(C_{out} - C_{in})\}, \quad (1)$$

where $k = -(\Delta V/V_0)/t$ is the shrinkage rate determined by exponential fits to the light-scattering data (26,28), SAV is the ratio of the initial vesicle surface

area (A_0) to the initial volume (V_0), V_W is the partial molar volume of water (18 cm^3/mol), and C_{in} (50 mM) and C_{out} (150 mM) are the initial concentrations of solute inside and outside the unilamellar vesicles (3,52). The light-scattering data were recorded with a time frame of 0–5 s and fit using Logger Pro 3.8 (Vernier Software, Beaverton, OR) as described in detail previously (26,28). An implicit assumption used here and in many previous studies (26,28,46–49,51–54) is that the change in intensity of the scattered light is proportional to the change in vesicle volume ($\Delta V/V_0$), although some studies use an additional quadratic term in the relationship between light scattering and vesicle volume (55,56). To check the effect of this quadratic term for our data, we determined shrinkage constants with or without this quadratic term. For bilayers containing similar concentrations of AQP4, we found that with or without the quadratic term, the ratios of the shrinkage constants were similar for comparisons of thick bilayers ((C22:1)(C22:1)PC, (C20:1)(C20:1)PC, or (C16:0)(C18:1)PC) to the thin bilayer ((C13:0)(C13:0)PC). For example, for protein/lipid mole ratios in the range 0.0027–0.0032, the ratio of shrinkage constant between our thickest ((C22:1)(C22:1)PC) and thinnest ((C13:0)(C13:0)PC) bilayer was 1.87 with the quadratic term and 1.81 without the quadratic term. Thus, in either case, the shrinkage constants were much greater for (C22:1)(C22:1)PC than for (C13:0)(C13:0)PC. The validity of the assumption that the change in scattered light intensity is proportional to $\Delta V/V_0$ is also indicated by the close agreement between the unit permeability results obtained by our osmotic stress measurements and MD simulations (see Fig. 5).

For each proteoliposome, the AQP4 single-channel unit water permeability (P_u), with units of cm^3/s, was determined from

$$P_u = p_f / SuD, \tag{2}$$

where SuD is the AQP4 channel density per unit surface area, calculated from the measured vesicle diameter, channel concentration, lipid concentration, and area per lipid molecule (A_m). For each of our bilayer systems, we used values of A_m from x-ray diffraction measurements of similar liquid-crystalline PC bilayers (43). Liposomes with the composition of the relevant proteoliposome were used as controls.

MD simulations

Simulation setup and preequilibration

The AQP4-M23 tetramer (PDB: 2D57) was embedded with the help of CHARMM-GUI (57) into two patches of membrane bilayers with different bilayer thicknesses. A thick membrane bilayer was composed of 247 long hydrocarbon chain lipids ((C22:1)(C22:1)PC), and a thin membrane bilayer was composed of 256 short hydrocarbon chain lipids ((C14:0)(C14:0)PC). There was no PG lipid in the simulation, with the assumption that a small portion of anionic lipids would not affect AQP4 function. Each system was solvated and 200 mM NaCl was added to the system, with the same ion concentration on either side of the membrane. Relaxation simulations were performed for both thick and thin membrane bilayers for 20 ns with the protein backbone fixed. Then, four 150 ns preequilibrium simulations for each membrane thickness were performed with no restraints (such as protein backbone restraints) under constant temperature (300 K) and constant pressure (1 atm). For both relaxation and preequilibrium simulations, particle-mesh Ewald (PME) (58) was used to evaluate long-range electrostatic interactions. The CHARMM (c36) force field (59,60) was applied to both lipid and protein. A modified TIP3P water model (59) in the CHARMM force field was used. The r-RESPA multiple-time-step integrator (61) was applied with time steps of 2 and 4 fs for short-range nonbonded and long-range electrostatic interactions, respectively. All simulations were carried out with the NAMD 2 (http://www.ks.uiuc.edu/Research/namd/2.9/ug/) (62).

Production simulations in the presence of an ion gradient across the membrane

During the 150 ns preequilibration simulations mentioned in the previous section, the AQP4-M23 protein adapts its conformation according to the different membrane thicknesses. Production simulations were then performed in the presence of an ion gradient across the membrane to study AQP4 water permeation in response to osmotic pressure. No restraint in the protein or membrane was employed in these simulations. To generate the ion gradient, extra ions were removed on either side of the membrane so that the NaCl ion concentrations were $C_{in} = 50$ mM on the cytoplasmic side and $C_{out} = 150$ mM on the extracellular side. Due to this asymmetric ion concentration, a simulation cell was used with periodicity only in the directions along the membrane surface, x and y, but not along the membrane normal direction, z. Instead of PME, the multilevel summation method (63) was applied to evaluate electrostatic interactions for the semiperiodic system. Unlike some previous studies on ion channels with asymmetric ion net charges across the membrane (64,65), no charge gradient was used here. An NVT ensemble was applied. Along the membrane normal (the z axis), the simulated system was confined at the lower and upper boundaries, $z = \pm a$, by a harmonic restoring potential. For this purpose, a containing force of magnitude $-k(z-a)$ for $z > a$, and $+k(z+a)$ for $z < -a$, was applied along the minus direction, implemented using the TclBC scriptable boundary condition feature of NAMD. The force constant was chosen to be $k = 3$ kcal/mol/Å^2. Twenty semiperiodic production simulations (five production simulations after each of the four preequilibrium simulations) were carried out for 40 ns for each membrane thickness in the presence of the ion gradient. Water permeation calculations and AQP4 structural analyses were performed from these 20 simulation trajectories for each membrane thickness. The AQP4 single-channel unit water permeability, P_u, was determined for each membrane thickness based on (66)

$$P_u = j_w / (C_{out} - C_{in}), \tag{3}$$

where j_W (mol/s) is the averaged net water flux through each AQP4 water channel, with each tetramer containing four channels (3).

Channel pore structure analysis

From the described semiperiodic simulation trajectories, AQP4 monomer structures were aligned for each membrane thickness and their root mean-square displacements (RMSDs) with regard to the crystal structure were determined. Based on the resulting RMSD values, the structures were classified into eight clusters, with an RMSD cutoff of 1.8 Å, employing g_cluster (67) in GROMACS (68). From the most populated cluster, i.e., representing a total probability of >60%, 50 central channel structures were taken out as representative structures for each membrane thickness. From these representative structures, water channel pore radii were computed with HOLE 2.0 (69) and averaged.

Comparison with bilayer hydrocarbon thicknesses

To relate the osmotic gradient and MD simulation results with bilayer hydrocarbon thicknesses, we employed data from x-ray scattering from fully hydrated PC multilayers (43) and diffraction measurements from oriented PC multilayers near full hydration (39), together with the assumption that the 20 mol % PGs used in the osmotic-gradient experiments did not appreciably change the d_{hc}. For d_{hc}, we used values of 3.44, 2.71, 2.54, and 2.41 nm for (C22:1)(C22:1)PC, (C16:0)(C18:1)PC, (C14:0)(C14:0)PC, and (C13:0)(C13:0)PC, respectively. For (C20:1)(C20:1)PC, we used a d_{hc} value of 3.07 nm, the average of (C22:1)(C22:1)PC (43) and (C18:1)(C18:1)PC (39), which should be an accurate estimate, as the hydrocarbon thickness for dimonounsaturated liquid-crystalline PC bilayers varies linearly with the number of carbon atoms (70). The bilayer thickness at each point of the membrane surface was measured and averaged over the last 20 ns of the MD simulation trajectory by a script analyzing local membrane properties (71).

RESULTS

Fig. 1 *a* shows typical osmotic-gradient-driven changes in the time course of light scattering for (C22:1)(C22:1)PC

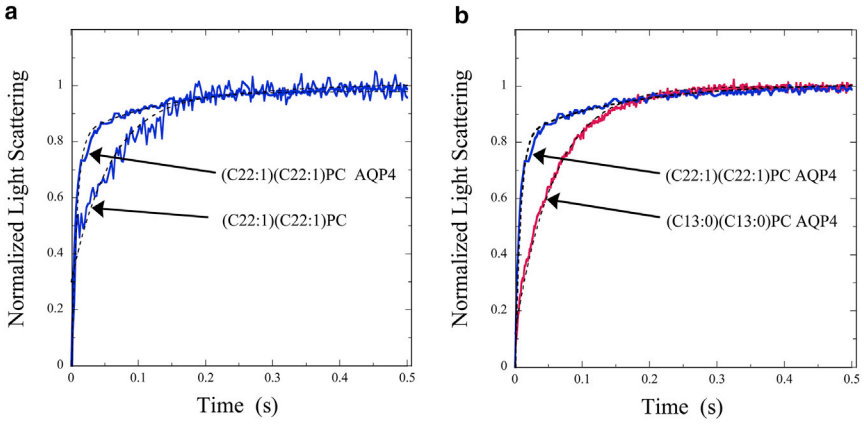

FIGURE 1 Solid curves show osmotic-gradient-driven changes in light scattering for (*a*) (C22:1)(C22:1)PC in the absence and presence of AQP4 (protein/lipid molar ratio of 0.0015) and (*b*) (C22:1)(C22:1)PC and (C13:0)(C13:0)PC bilayers containing AQP4 (both at protein/lipid molar ratios of 0.0015). In all cases the osmotic gradient was applied at time $t = 0$, and traces were put on the same relative scale by normalizing the light scattering to go from 0 at time $t = 0$ to 1 when the scattering leveled off. Exponential fits to the data are shown with dashed black lines.

in the absence and presence of AQP4. For each trace, light scattering increased sharply after the osmotic gradient was applied at time t = 0, and then eventually leveled off. However, the rate of change was increased by the addition of AQP4, indicating that this protein increased vesicle water permeability. Fig. 1 *b* shows light-scattering data for (C22:1)(C22:1)PC and (C13:0)(C13:0)PC with the same AQP4/lipid molar ratio. In these traces, the rate of light-scattering change was larger for AQP4 in (C22:1)(C22:1)PC than in (C13:0)(C13:0)PC, indicating smaller water permeability for the latter type of proteoliposome.

Similar experiments, together with Eq. 1, were used to calculate water permeabilities (p_f) for a wide range of AQP4 protein/lipid (P/L) ratios in (C22:1)(C22:1)PC, (C20:1)(C20:1)PC, (C16:0)(C18:1)PC, and (C13:0)(C13:0)PC proteoliposomes, as well as for protein-free liposomes (Fig. 2). The p_f values for the liposomes were 0.014 cm/s, 0.016 cm/s, 0.015 cm/s, and 0.017 cm/s for (C22:1)(C22:1)PC, (C20:1)(C20:1)PC, (C16:0)(C18:1)PC, and (C13:0)(C13:0)PC, respectively. For each of these lipid systems, p_f increased linearly with increasing P/L ratio. However, the slope of the p_f versus P/L relation depended on the lipid, with the smallest slope observed for (C13:0)(C13:0)PC (Fig. 2).

These p_f data were used with Eq. 2 to calculate the single-channel (unit) water permeability (P_u) for AQP4 in each of these lipid systems. Values of P_u were $3.5 \pm 0.2 \times 10^{-13}$ cm^3/s (mean ± SE), $3.0 \pm 0.3 \times 10^{-13}$ cm^3/s, $2.5 \pm 0.2 \times 10^{-13}$ cm^3/s, and $0.9 \pm 0.1 \times 10^{-13}$ cm^3/s in bilayers containing (C22:1)(C22:1)PC, (C20:1)(C20:1)PC, (C16:0)(C18:1)PC, and (C13:0)(C13:0)PC, respectively. Thus, a strong dependency of single-channel permeability on the bilayer composition was found, with P_u being largest in (C22:1)(C22:1)PC and smallest in (C13:0)(C13:0)PC bilayers (Fig. 3).

To investigate the molecular origin of the observed bilayer thickness effects on AQP4 water permeability, MD simulations were performed on AQP4 tetramers in membrane bilayers of two thicknesses, (C22:1)(C22:1)PC and (C14:0)(C14:0)PC. All of the MD simulation structures are shown in views parallel to the plane of the membrane, with the extracellular surface at the top of the figure.

In the presence of the osmotic gradient across the membrane, water molecules moved mostly single file through each AQP4 water channel (Fig. 4). Net water flux was determined and water permeation, P_u, was calculated from Eq. 3. The resulting values of P_u were $3.3 \pm 0.1 \times 10^{-13}$ cm^3/s and $2.5 \pm 0.1 \times 10^{-13}$ cm^3/s for (C22:1)(C22:1)PC and (C14:0)(C14:0)PC bilayers, respectively.

The relationship of AQP4 water permeability to bilayer hydrocarbon thickness, d_{hc}, is shown in Fig. 5. The values of P_u obtained from the osmotic-gradient experiments and from the simulations agreed with each other. P_u decreased with decreasing values of d_{hc}, so that the values were

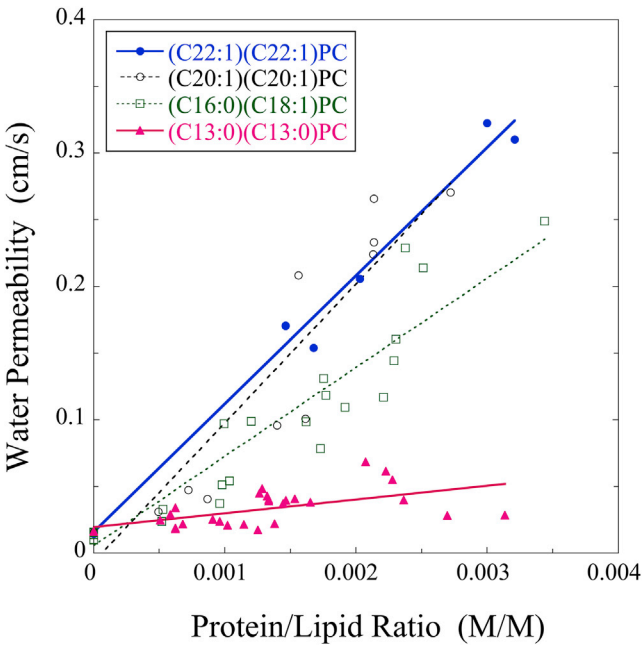

FIGURE 2 Water permeabilities (p_f) for AQP4 measured as a function of protein/lipid molar ratio in (C22:1)(C22:1)PC, (C20:1:C20:1)PC, (C16:0)(C18:1)PC, and (C13:0)(C13:0)PC.

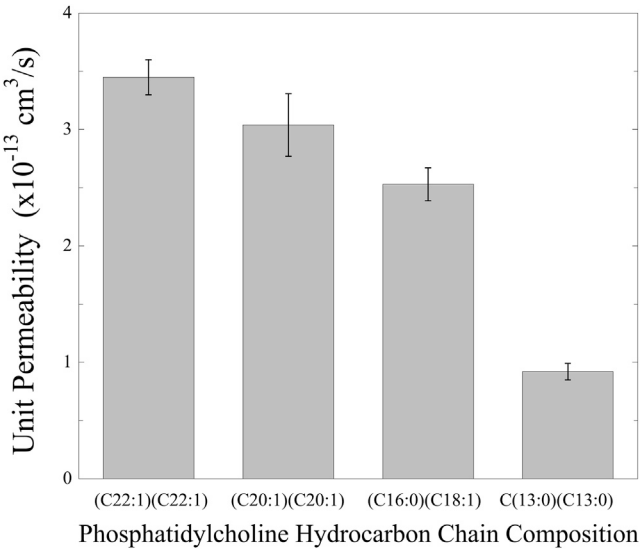

FIGURE 3 Single-channel (unit) water permeabilities (mean ± SE) measured for AQP4 in bilayers with the lipid compositions shown in Fig. 2. The difference in unit permeability was statistically significant between (C22:1)(C22:1)PC and (C13:0)(C13:0)PC, with a t probability of $t < 0.0001$ by Welch's t-test, whereas the t probability was 0.0979 between (C22:1)(C22:1)PC and(C20:1)(C20:1)PC.

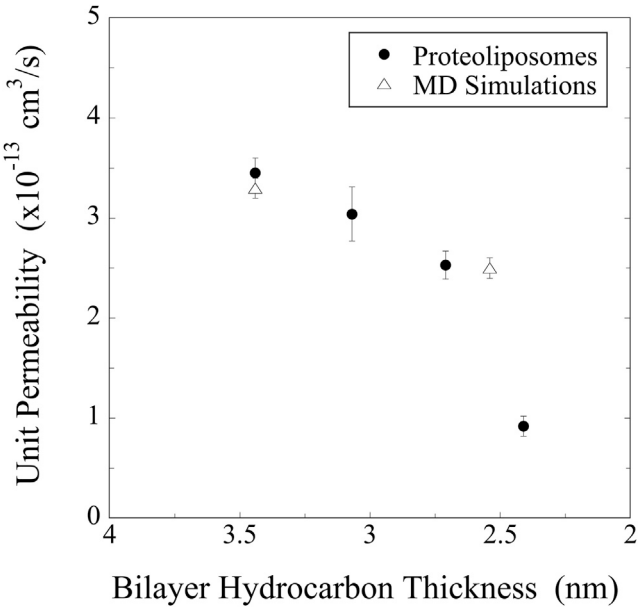

FIGURE 5 AQP4 single-channel (unit) water permeabilities (mean ± SE) determined by osmotic-gradient experiments with proteoliposomes (*solid circles*) and by MD simulations (*open triangles*) plotted versus bilayer hydrocarbon thickness. The lipid compositions are given in the caption to Fig. 2 for the osmotic-gradient experiments and are C(22:1)(22:1)PC and (C14:0)(C14:0)PC for the simulations.

significantly smaller at $d_{hc} = 2.4$ nm than at larger hydrocarbon thicknesses.

The MD simulations (Figs. 6, 7, 8, and 9) provide atomic details on modifications in AQP4 molecular organization with changing bilayer thickness. An AQP4 water channel has an hourglass shape (50), with a narrow region in the middle of the pore (10 Å $> z >$ −15 Å) and funnel-shaped entrances (vestibules) located at both ends of the pore ($z >$ 10 Å and $z <$ −15 Å) (Fig. 7). The water selectivity filter and NPA residues that, together with the internal quadrupolar AQP electrostatic field, cause orientation of water molecules passing through the channel (72,73), are both located in the narrow region near the middle of the pore (50,74). Compared to the (C22:1)(C22:1)PC bilayer, for the (C14:0)(C14:0)PC bilayer, the simulations suggested that there were very small changes both in protein organization and pore radius near the selectivity filter (near $z =$ 10 Å), NPA residues (near $z = 0$), or in the extracellular

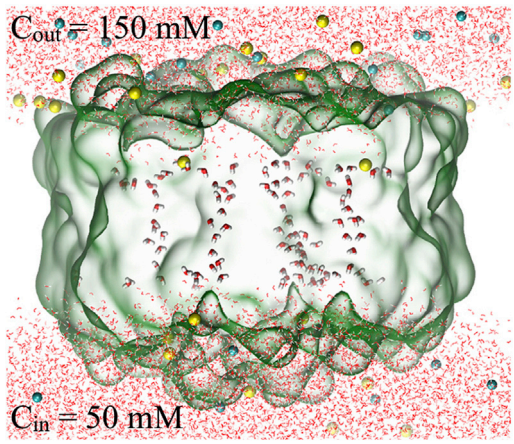

FIGURE 4 The simulated system in a view parallel to the plane of the bilayer. A semiperiodic simulation was carried out with periodicity only in the directions along the membrane surface, but not along the membrane normal direction, to maintain an asymmetric ion concentration across the bilayer. The AQP4 tetramer is shown as a green surface, with four single-file water chains in each tetramer. Na^+ and Cl^- ions are shown as yellow and blue spheres, respectively. For clarity, membrane lipids are not shown.

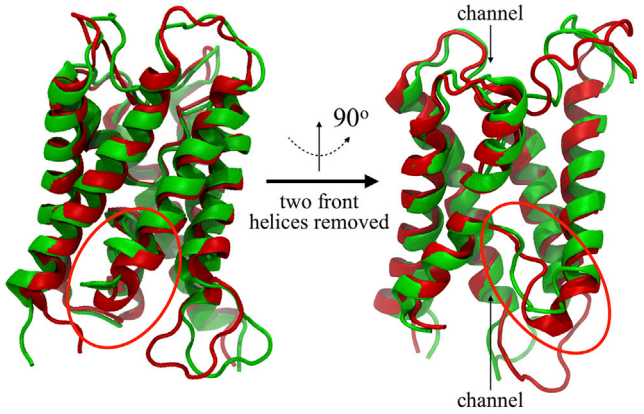

FIGURE 6 Monomer structures of AQP4 in different membranes in two views rotated 90° in the plane of the membrane. The channel colored in green was embedded in a (C14:0)(C14:0)PC bilayer, whereas the red channel was embedded in a (C22:1)(22:1)PC bilayer. The arrows point down the middle of the channel. A red circle highlights the major differences in structure between AQP4 in these bilayers.

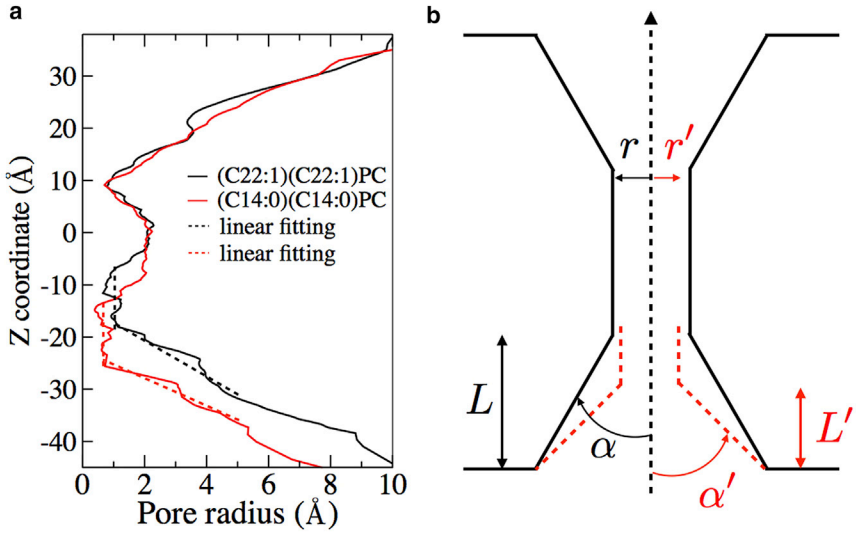

FIGURE 7 Geometrical characteristics of the AQP4 channel. (*a*) Tthe AQP4 channel radius averaged over 20 MD simulations (*solid lines*) for two different membrane bilayer thicknesses. Negative z values correspond to the cytoplasmic side of the membrane; the cytoplasmic channel entrance is located at $z < -15$ Å, the NPA residues are near $z = 0$ Å, and the selectivity filter is near $z = +10$ Å. The channel entrance structural parameters (entrance angle, depth, and pore radius) were measured from linear fitting (*dashed lines*) of the channel entrance radius. (*b*) Schematic plot illustrating the narrowing of the channel entrance in a thin bilayer (*red dashed lines*) compared to a thick bilayer (*black lines*) near the cytoplasmic entrance (*bottom of drawing*).

entrance ($z > 10$ Å). However, relatively large changes in the length of the helices near the cytoplasmic entrance were observed in the simulations in the thinner bilayer (Fig. 6). Specifically, the adjacent loop moved closer to the water channel at the cytoplasmic entrance region ($z < -15$ Å) in the thin bilayer ((C14:0)(C14:0)PC) than in the thick bilayer ((C22:1)(C22:1)PC). The AQP4 structures in these bilayers (Fig. 6) showed differences in AQP4 water pore radii between the NPA residues and the cytoplasmic entrance (near $z = -7$ Å) and in the cytoplasmic entrance ($z < -15$ Å). The pore radius was larger for the thin bilayer near $z = -7$ Å, whereas in the cytoplasmic entrance region ($z < -15$ Å), the thin bilayer had a smaller pore radius, a longer pore length, a shallower entrance, and a larger entrance angle (Fig. 7). In the thinner ((C14:0)(C14:0)PC) bilayer, the water channel-pore entrance became steeper, longer, and narrower compared to the thicker bilayer ((C22:1)(C22:1)PC) (Fig. 7). In the (C14:0)(C14:0)PC bilayer, the radius of the cytoplasmic water channel entrance from $z = -25$ Å to $z = -15$ Å was even smaller than the pore radius near the NPA residues in the middle of the pore (Fig. 7 *a*).

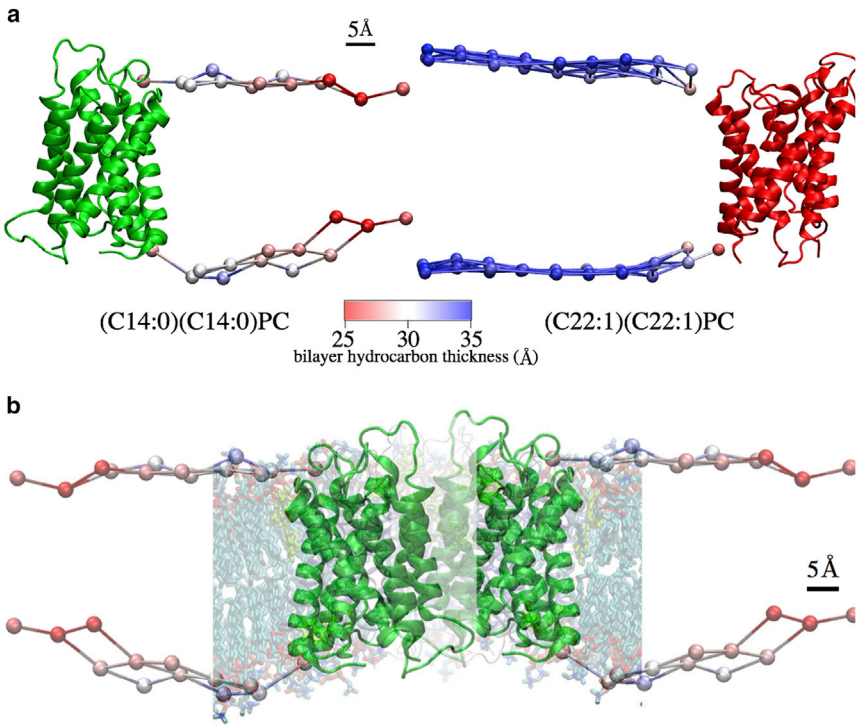

FIGURE 8 Comparison of bilayer thicknesses around the AQP4 channel. Meshed surfaces indicate simulation-trajectory-averaged positions of phosphorus atoms in the upper (extracellular) and lower (cytoplasmic) leaflets. (*a*) Hydrocarbon thicknesses are indicated by colors on the surface beads in the presence of AQP4 (*green*, (C14:0)(C14:0)PC; *red*, (C22:1)(22:1)PC). (*b*) Predicted thickness of the (C14:0)(C14:0)PC bilayer near the protein.

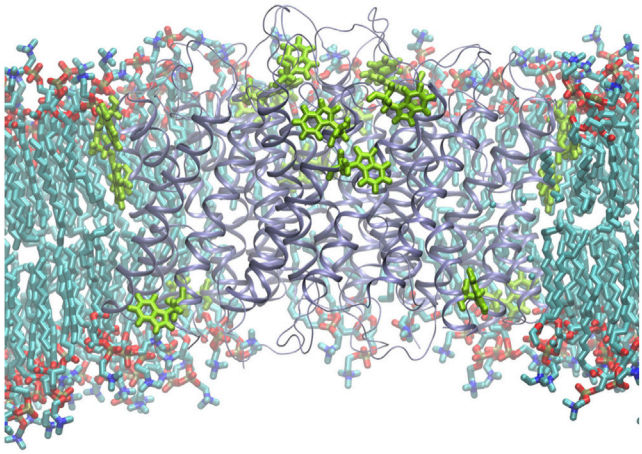

FIGURE 9 The locations of Trp residues (*light green*) are shown in a typical snapshot of AQP4 in the thin (C14:0)(C14:0)PC bilayer at the end of an equilibrated MD simulation. The bilayer is distorted due to the hydrophobic mismatch between protein and bilayer (see Fig. 8 *b*).

These structural modifications of the AQP4 channel could be a result of strong hydrophobic mismatch between the membrane bilayer and the protein. The length of the protein is larger than the thickness of the (C14:0)(C14:0)PC bilayer, but is only slightly smaller than the thickness of the (C22:1)(C22:1)PC bilayer (Fig. 8 *a*). As a result, a difference in membrane bilayer thickness was observed between membrane regions close to the protein and regions >30 Å away in (C14:0)(C14:0)PC (Fig. 8, *a* and *b*); this bilayer became much thicker (up to ~5 Å) as it got closer to AQP4. The increase in bilayer thickness close to AQP4 indicated the presence of membrane stress applied to the channels, which resulted in changes in AQP4 channel structure.

An intriguing observation of the MD simulations was that in the thin bilayer, where there was a large hydrophobic mismatch (Fig. 8), AQP4 sat closer to the upper (extracellular) membrane-water interface than to the lower (cytoplasmic) interface. We argue that this could be the result of the asymmetric distribution in AQP4 of the tryptophan (Trp) residues, which preferentially locate at membrane-water interfaces (75). Fig. 9 shows that there were 12 Trps in the upper part of the protein, but only four Trps in the lower part (Fig. 9), and thus, AQP4 was located closer to the upper (extracellular) interface than to the lower (cytoplasmic) interface.

DISCUSSION

The functions of several ion channels are modified by changes in thickness of the membrane lipid bilayer (21,24,34,36–38,76–84). Aquaporins are specialized for the selective permeability across membranes of water (and glycerol in the case of aquaglyceroporins) and exclude ions (1–4,50,85). Here, we showed that the water permeability of the AQP4 channel depended strongly on bilayer thickness. Bilayers composed of the various phosphatidylcholines used here all have similar elastic stretch moduli (a measure of bilayer elasticity), in the range 234–265 mN/m (39). This implies that, for the bilayer systems in this study, differences in bilayer elasticity should not be a major factor in the observed differences in channel water permeability.

For a given bilayer thickness, our osmotic pressure measurements and MD simulations gave very similar values for AQP4 single-channel water permeability (Fig. 5). Moreover, both techniques also showed that P_u depended on the width of the hydrocarbon chain region of the bilayer. A thin membrane bilayer did not affect the structure of AQP4 near its selectivity filter (Figs. 6 and 7 *a*), which might indicate that there was little effect of membrane thickness on channel selectivity. However, the simulation results suggested that changes in bilayer thickness affected both the structure of the AQP4 cytoplasmic vestibule and the length of the small-radius pore region of the channel (Figs. 6 and 7). As discussed below, either, or a combination, of these structural changes could explain the decreased water permeability with smaller bilayer hydrocarbon thickness (Fig. 5).

The structural modification of the cytoplasmic entrance caused by short phospholipid chain length could be a molecular origin for the AQP4 water permeation decrease. As detailed in the recent theoretical modeling of AQPs by Gravelle and colleagues (40), the entrance effect could be a limiting factor for water conductance through AQP channels. In an hourglass-shaped channel, water permeation decreases when the entrance angle, α, becomes larger ($\alpha > 7^\circ$) and when the ratio of the entrance depth to the pore radius (L/r) becomes smaller (40). Our simulation results were in close agreement with this theory (Fig. 7). In the thin (C14:0)(C14:0)PC bilayer, the AQP4 water channel entrance changed its angle from 13° to 23°, entrance depth from 18 Å to 10 Å, and pore radius from 1.0 Å to 0.7 Å. With such changes in the channel's entrance structure, the theory predicts a 1.4-fold decrease in water permeation (40), which is in close agreement with the 1.3-fold decrease predicted in our simulation between thick ((C22:1)(C22:1)PC)and thin ((C14:0)(C14:0)PC) bilayers, as well as in our osmotic-gradient experiments between (C22:1)(C22:1)PC and the (C16:0)(C18:1)PC bilayer, which has a thickness similar to that of (C14:0)(C14:0)PC (Fig. 5). However, this is much smaller than the 3.9-fold decrease observed in the osmotic-gradient experiments between (C22:1)(C22:1)PC and the even thinner (C13:0)(C13:0)PC bilayer (Fig. 5).

Besides the channel entrance effect, there are other factors that could cause the small water permeability in the thin bilayers. As the pore radius is slightly decreased, water conductance across the restriction zone (pore radius <1 Å) could also contribute to the decrease in permeation. Furthermore, the elongation of the channel region in the thin membrane (Fig. 7) could increase the interaction between water and the channel and also increase the length of the water chain, thereby increasing channel water resistance.

These results suggest that the AQP4 channel is constructed to provide maximum water permeability in bilayers with thicknesses found in nature. Specifically, the channel permeability became markedly smaller for a hydrocarbon thickness of <2.5 nm (Fig. 5), which is thinner than that typically found in biological membranes (31).

Although our data demonstrated that the function of AQP4 depended on membrane bilayer thickness, our results also showed the robustness of the channel, as previously reported for AQP channels (86). That is, AQP4 allowed water passage over the wide range of bilayer thicknesses studied here. More importantly, in the MD simulations, no appreciable conformation changes were observed in key channel regions, such as near the selectivity filter motif or the NPA motif (Figs. 6 and 7), indicating few effects on channel selectivity. Only the detailed structure of AQP4 near the cytoplasmic vestibule changed appreciably with decreasing bilayer thickness (Figs. 5 and 6).

Finally, we return to the effects of membrane cholesterol on AQP4 permeability function. We argue that specific cholesterol-AQP4 interactions do not make a dominant contribution to the total effect, because P_u is quite different for 1:1 sphingomyelin/cholesterol and 1:1 (C16:0)(C18:1) PC/cholesterol bilayers at the same cholesterol/AQP4 ratio (28). As noted in the Introduction, in addition to increasing bilayer thickness, cholesterol also modifies bilayer elasticity, as indicated by cholesterol-induced increases in the bilayer area compressibility modulus (K_A), which is much larger for 1:1 sphingomyelin/cholesterol than for 1:1 (C16:0)(C18:1)PC/cholesterol bilayers (31,87). We found that P_u was extremely low ($0.3 \pm 0.1 \times 10^{-13}$ cm^3/s) for AQP4 in equimolar sphingomyelin and cholesterol bilayers (31), even though the bilayer hydrocarbon thickness of a 1:1 sphingomyelin/cholesterol bilayer (3.6 nm) is comparable to the thickest bilayers used in this study (Fig. 5). Thus, although, as shown here, thickness changes modify AQP4 permeability, the dominant effect of cholesterol on AQP4 function is likely due to cholesterol's altering membrane elasticity. Molecular details for AQP4 permeability changes as a function of bilayer elasticity are not known at present.

AUTHOR CONTRIBUTIONS

J.T. made the proteoliposomes and performed the osmotic gradient experiments; Z.W. performed the MD simulations; M.M.B. helped express and purify AQP4-M23; K.S. designed the MD simulations and helped analyze the MD results; T.J.M. designed the research, particularly the osmotic gradient experiments; T.J.M. and Z.W. wrote the original draft of the manuscript; and M.M.B. and K.S. contributed to the writing.

ACKNOWLEDGMENTS

We thank Dr. Peter Agre for supplying plasmids, Dr. Harold Erickson for the use of the French press, Dr. Terrence Oas for use of the stopped-flow apparatus, Dr. David Needham for use of the quasielastic light-scattering equipment, and Drs. Jennifer Carbrey, Sidney Simon, David Hardy, and Emad Tajkhorshid for many helpful suggestions.

This work was supported by grants R01-GM27278, 5R01-GM098243-02, R01-GM067887, and U54GM087519 from the National Institutes of Health, and PHY1430124 from the National Science Foundation. The authors also acknowledge supercomputer time on Stampede at the Texas Advanced Computing Center (TACC), provided by grant MCA93S028 from the Extreme Science and Engineering Discovery Environment (XSEDE), which is supported by the National Science Foundation (OCI-1053575).

REFERENCES

1. Agre, P., and D. Kozono. 2003. Aquaporin water channels: molecular mechanisms for human diseases. *FEBS Lett.* 555:72–78.
2. King, L. S., D. Kozono, and P. Agre. 2004. From structure to disease: the evolving tale of aquaporin biology. *Nat. Rev. Mol. Cell Biol.* 5:687–698.
3. Borgnia, M., S. Nielsen, …, P. Agre. 1999. Cellular and molecular biology of the aquaporin water channels. *Annu. Rev. Biochem.* 68:425–458.
4. Venero, J. L., A. Machado, and J. Cano. 2004. Importance of aquaporins in the physiopathology of brain edema. *Curr. Pharm. Des.* 10:2153–2161.
5. Verkman, A. S. 2002. Physiological importance of aquaporin water channels. *Ann. Med.* 34:192–200.
6. Amiry-Moghaddam, M., A. Williamson, …, O. P. Ottersen. 2003. Delayed K^+ clearance associated with aquaporin-4 mislocalization: phenotypic defects in brains of α-syntrophin-null mice. *Proc. Natl. Acad. Sci. USA.* 100:13615–13620.
7. Badaut, J., J. F. Brunet, and L. Regli. 2007. Aquaporins in the brain: from aqueduct to "multi-duct". *Metab. Brain Dis.* 22:251–263.
8. Benfenati, V., M. Caprini, …, M. Amiry-Moghaddam. 2011. An aquaporin-4/transient receptor potential vanilloid 4 (AQP4/TRPV4) complex is essential for cell-volume control in astrocytes. *Proc. Natl. Acad. Sci. USA.* 108:2563–2568.
9. Bloch, O., and G. T. Manley. 2007. The role of aquaporin-4 in cerebral water transport and edema. *Neurosurg. Focus.* 22:E3.
10. Fenton, R. A., H. B. Moeller, …, N. MacAulay. 2010. Differential water permeability and regulation of three aquaporin 4 isoforms. *Cell. Mol. Life Sci.* 67:829–840.
11. Jung, J. S., R. V. Bhat, …, P. Agre. 1994. Molecular characterization of an aquaporin cDNA from brain: candidate osmoreceptor and regulator of water balance. *Proc. Natl. Acad. Sci. USA.* 91:13052–13056.
12. Manley, G. T., D. K. Binder, …, A. S. Verkman. 2004. New insights into water transport and edema in the central nervous system from phenotype analysis of aquaporin-4 null mice. *Neuroscience.* 129:983–991.
13. Nicchia, G. P., M. Srinivas, …, D. C. Spray. 2005. New possible roles for aquaporin-4 in astrocytes: cell cytoskeleton and functional relationship with connexin43. *FASEB J.* 19:1674–1676.
14. Pasantes-Morales, H., and S. Cruz-Rangel. 2010. Brain volume regulation: osmolytes and aquaporin perspectives. *Neuroscience.* 168:871–884.
15. Verkman, A. S., D. K. Binder, …, M. C. Papadopoulos. 2006. Three distinct roles of aquaporin-4 in brain function revealed by knockout mice. *Biochim. Biophys. Acta.* 1758:1085–1093.
16. Frydenlund, D. S., A. Bhardwaj, …, M. Amiry-Moghaddam. 2006. Temporary loss of perivascular aquaporin-4 in neocortex after transient middle cerebral artery occlusion in mice. *Proc. Natl. Acad. Sci. USA.* 103:13532–13536.
17. Saini, H., G. Fernandez, …, M. Levy. 2010. Differential expression of aquaporin-4 isoforms localizes with neuromyelitis optica disease activity. *J. Neuroimmunol.* 221:68–72.
18. Kanzaki, M., H. Mochizuki, …, K. Kamakura. 2008. Clinical features of opticospinal multiple sclerosis with anti-aquaporin 4 antibody. *Eur. Neurol.* 60:37–42.

19. Johannsson, A., G. A. Smith, and J. C. Metcalfe. 1981. The effect of bilayer thickness on the activity of $(Na^+ + K^+)$-ATPase. *Biochim. Biophys. Acta.* 641:416–421.
20. Mouritsen, O. G., and M. Bloom. 1984. Mattress model of lipid-protein interactions in membranes. *Biophys. J.* 46:141–153.
21. Andersen, O. S., and R. E. Koeppe, 2nd. 2007. Bilayer thickness and membrane protein function: an energetic perspective. *Annu. Rev. Biophys. Biomol. Struct.* 36:107–130.
22. Levitan, I., Y. Fang, …, V. Romanenko. 2010. Cholesterol and ion channels. *Subcell. Biochem.* 51:509–549.
23. McIntosh, T. J., and S. A. Simon. 2006. Roles of bilayer material properties in function and distribution of membrane proteins. *Annu. Rev. Biophys. Biomol. Struct.* 35:177–198.
24. Phillips, R., T. Ursell, …, P. Sens. 2009. Emerging roles for lipids in shaping membrane-protein function. *Nature.* 459:379–385.
25. Syeda, R., J. S. Santos, and M. Montal. 2014. Lipid bilayer modules as determinants of K^+ channel gating. *J. Biol. Chem.* 289:4233–4243.
26. Tong, J., J. T. Canty, …, T. J. McIntosh. 2013. The water permeability of lens aquaporin-0 depends on its lipid bilayer environment. *Exp. Eye Res.* 113:32–40.
27. Lundbaek, J. A., P. Birn, …, O. S. Andersen. 2005. Capsaicin regulates voltage-dependent sodium channels by altering lipid bilayer elasticity. *Mol. Pharmacol.* 68:680–689.
28. Tong, J., M. M. Briggs, and T. J. McIntosh. 2012. Water permeability of aquaporin-4 channel depends on bilayer composition, thickness, and elasticity. *Biophys. J.* 103:1899–1908.
29. O'Connor, J. W., and J. B. Klauda. 2011. Lipid membranes with a majority of cholesterol: applications to the ocular lens and aquaporin 0. *J. Phys. Chem. B.* 115:6455–6464.
30. McIntosh, T. J. 2007. X-ray diffraction to determine the thickness of raft and nonraft bilayers. *Methods Mol. Biol.* 398:221–230.
31. Rawicz, W., B. A. Smith, …, E. Evans. 2008. Elasticity, strength, and water permeability of bilayers that contain raft microdomain-forming lipids. *Biophys. J.* 94:4725–4736.
32. Martinac, B., and O. P. Hamill. 2002. Gramicidin A channels switch between stretch activation and stretch inactivation depending on bilayer thickness. *Proc. Natl. Acad. Sci. USA.* 99:4308–4312.
33. Mobashery, N., C. Nielsen, and O. S. Andersen. 1997. The conformational preference of gramicidin channels is a function of lipid bilayer thickness. *FEBS Lett.* 412:15–20.
34. Goforth, R. L., A. K. Chi, …, O. S. Andersen. 2003. Hydrophobic coupling of lipid bilayer energetics to channel function. *J. Gen. Physiol.* 121:477–493.
35. Kim, T., K. I. Lee, …, W. Im. 2012. Influence of hydrophobic mismatch on structures and dynamics of gramicidin a and lipid bilayers. *Biophys. J.* 102:1551–1560.
36. Garavaglia, M., S. Dopinto, …, M. Paulmichl. 2004. Membrane thickness changes ion-selectivity of channel-proteins. *Cell. Physiol. Biochem.* 14:231–240.
37. Rusinova, R., D. M. Kim, …, O. S. Andersen. 2014. Regulation of ion channel function by the host lipid bilayer examined by a stopped-flow spectrofluorometric assay. *Biophys. J.* 106:1070–1078.
38. Yuan, C., R. J. O'Connell, …, S. N. Treistman. 2007. Regulation of the gating of BKCa channel by lipid bilayer thickness. *J. Biol. Chem.* 282:7276–7286.
39. Rawicz, W., K. C. Olbrich, …, E. Evans. 2000. Effect of chain length and unsaturation on elasticity of lipid bilayers. *Biophys. J.* 79:328–339.
40. Gravelle, S., L. Joly, …, L. Bocquet. 2013. Optimizing water permeability through the hourglass shape of aquaporins. *Proc. Natl. Acad. Sci. USA.* 110:16367–16372.
41. Yukutake, Y., S. Tsuji, …, M. Suematsu. 2008. Mercury chloride decreases the water permeability of aquaporin-4-reconstituted proteoliposomes. *Biol. Cell.* 100:355–363.
42. Kučerka, N., B. W. Holland, …, J. Katsaras. 2012. Scattering density profile model of POPG bilayers as determined by molecular dynamics simulations and small-angle neutron and x-ray scattering experiments. *J. Phys. Chem. B.* 116:232–239.
43. Kucerka, N., S. Tristram-Nagle, and J. F. Nagle. 2005. Structure of fully hydrated fluid phase lipid bilayers with monounsaturated chains. *J. Membr. Biol.* 208:193–202.
44. Tong, J., M. M. Briggs, …, T. J. McIntosh. 2009. Sorting of lens aquaporins and connexins into raft and nonraft bilayers: role of protein homo-oligomerization. *Biophys. J.* 97:2493–2502.
45. Chen, P. S., Jr., T. Y. Toribara, and H. Warner. 1956. Microdetermination of phosphorus. *Anal. Chem.* 28:1756–1758.
46. Carbrey, J. M., D. A. Gorelick-Feldman, …, P. Agre. 2003. Aquaglyceroporin AQP9: solute permeation and metabolic control of expression in liver. *Proc. Natl. Acad. Sci. USA.* 100:2945–2950.
47. Liu, K., H. Nagase, …, P. Agre. 2006. Purification and functional characterization of aquaporin-8. *Biol. Cell.* 98:153–161.
48. Yakata, K., K. Tani, and Y. Fujiyoshi. 2011. Water permeability and characterization of aquaporin-11. *J. Struct. Biol.* 174:315–320.
49. Kozono, D., X. Ding, …, Y. Kitagawa. 2003. Functional expression and characterization of an archaeal aquaporin. AqpM from *Methanothermobacter marburgensis*. *J. Biol. Chem.* 278:10649–10656.
50. Ho, J. D., R. Yeh, …, R. M. Stroud. 2009. Crystal structure of human aquaporin 4 at 1.8 Å and its mechanism of conductance. *Proc. Natl. Acad. Sci. USA.* 106:7437–7442.
51. Yang, B., A. N. van Hoek, and A. S. Verkman. 1997. Very high single-channel water permeability of aquaporin-4 in baculovirus-infected insect cells and liposomes reconstituted with purified aquaporin-4. *Biochemistry.* 36:7625–7632.
52. Kai, L., R. Kaldenhoff, …, Z. Xu. 2010. Preparative scale production of functional mouse aquaporin 4 using different cell-free expression modes. *PLoS One.* 5:e12972.
53. Werten, P. J., L. Hasler, …, P. M. Deen. 2001. Large-scale purification of functional recombinant human aquaporin-2. *FEBS Lett.* 504:200–205.
54. Borgnia, M. J., D. Kozono, …, P. Agre. 1999. Functional reconstitution and characterization of AqpZ, the *E. coli* water channel protein. *J. Mol. Biol.* 291:1169–1179.
55. Illsley, N. P., and A. S. Verkman. 1986. Serial permeability barriers to water transport in human placental vesicles. *J. Membr. Biol.* 94:267–278.
56. Horner, A., F. Zocher, …, P. Pohl. 2015. The mobility of single-file water molecules is governed by the number of H-bonds they may form with channel-lining residues. *Sci. Adv.* 1:e1400083.
57. Jo, S., T. Kim, …, W. Im. 2008. CHARMM-GUI: a web-based graphical user interface for CHARMM. *J. Comput. Chem.* 29:1859–1865.
58. Essmann, U., L. Perera, …, L. G. Pedersen. 1995. A smooth particle mesh Ewald method. *J. Chem. Phys.* 103:8577–8593.
59. MacKerell, A. D., D. Bashford, …, M. Karplus. 1998. All-atom empirical potential for molecular modeling and dynamics studies of proteins. *J. Phys. Chem. B.* 102:3586–3616.
60. Klauda, J. B., R. M. Venable, …, R. W. Pastor. 2010. Update of the CHARMM all-atom additive force field for lipids: validation on six lipid types. *J. Phys. Chem. B.* 114:7830–7843.
61. Tuckerman, M., B. J. Berne, and G. J. Martyna. 1992. Reversible multiple time scale molecular dynamics. *J. Chem. Phys.* 97:1990–2001.
62. Phillips, J. C., R. Braun, …, K. Schulten. 2005. Scalable molecular dynamics with NAMD. *J. Comput. Chem.* 26:1781–1802.
63. Hardy, D. J., Z. Wu, …, K. Schulten. 2015. Multilevel summation method for electrostatic force evaluation. *J. Chem. Theory Comput.* 11:766–779.
64. Treptow, W., M. Tarek, and M. L. Klein. 2009. Initial response of the potassium channel voltage sensor to a transmembrane potential. *J. Am. Chem. Soc.* 131:2107–2109.
65. Gurtovenko, A. A., and I. Vattulainen. 2005. Pore formation coupled to ion transport through lipid membranes as induced by transmembrane

ionic charge imbalance: atomistic molecular dynamics study. *J. Am. Chem. Soc.* 127:17570–17571.

66. Zhu, F., E. Tajkhorshid, and K. Schulten. 2004. Theory and simulation of water permeation in aquaporin-1. *Biophys. J.* 86:50–57.
67. Daura, X., K. Gademann, …, A. E. Mark. 1999. Peptide folding: when simulation meets experiment. *Angew. Chem. Int. Ed. Engl.* 38:236–240.
68. Hess, B., C. Kutzner, …, E. Lindahl. 2008. GROMACS 4: algorithms for highly efficient, load-balanced, and scalable molecular simulation. *J. Chem. Theory Comput.* 4:435–447.
69. Smart, O. S., J. M. Goodfellow, and B. A. Wallace. 1993. The pore dimensions of gramicidin A. *Biophys. J.* 65:2455–2460.
70. Lewis, B. A., and D. M. Engelman. 1983. Lipid bilayer thickness varies linearly with acyl chain length in fluid phosphatidylcholine vesicles. *J. Mol. Biol.* 166:211–217.
71. Gapsys, V., B. L. de Groot, and R. Briones. 2013. Computational analysis of local membrane properties. *J. Comput. Aided Mol. Des.* 27:845–858.
72. Tajkhorshid, E., P. Nollert, …, K. Schulten. 2002. Control of the selectivity of the aquaporin water channel family by global orientational tuning. *Science.* 296:525–530.
73. de Groot, B. L., and H. Grubmüller. 2005. The dynamics and energetics of water permeation and proton exclusion in aquaporins. *Curr. Opin. Struct. Biol.* 15:176–183.
74. Tani, K., T. Mitsuma, …, Y. Fujiyoshi. 2009. Mechanism of aquaporin-4's fast and highly selective water conduction and proton exclusion. *J. Mol. Biol.* 389:694–706.
75. Yau, W.-M., W. C. Wimley, …, S. H. White. 1998. The preference of tryptophan for membrane interfaces. *Biochemistry.* 37:14713–14718.
76. Andersen, O. S., M. J. Bruno, …, R. E. Koeppe, 2nd. 2007. Single-molecule methods for monitoring changes in bilayer elastic properties. *Methods Mol. Biol.* 400:543–570.
77. Debret, G., H. Valadié, …, C. Etchebest. 2008. New insights of membrane environment effects on MscL channel mechanics from theoretical approaches. *Proteins.* 71:1183–1196.
78. Elliott, J. R., D. Needham, …, D. A. Haydon. 1983. The effects of bilayer thickness and tension on gramicidin single-channel lifetime. *Biochim. Biophys. Acta.* 735:95–103.
79. Hamill, O. P., and B. Martinac. 2001. Molecular basis of mechanotransduction in living cells. *Physiol. Rev.* 81:685–740.
80. Lundbaek, J. A. 2008. Lipid bilayer-mediated regulation of ion channel function by amphiphilic drugs. *J. Gen. Physiol.* 131:421–429.
81. O'Connell, R. J., C. Yuan, …, S. N. Treistman. 2006. Gating and conductance changes in BK(Ca) channels in bilayers are reciprocal. *J. Membr. Biol.* 213:143–153.
82. Perozo, E., A. Kloda, …, B. Martinac. 2002. Physical principles underlying the transduction of bilayer deformation forces during mechanosensitive channel gating. *Nat. Struct. Biol.* 9:696–703.
83. Balleza, D. 2012. Mechanical properties of lipid bilayers and regulation of mechanosensitive function: from biological to biomimetic channels. *Channels (Austin).* 6:220–233.
84. Suchyna, T. M., S. E. Tape, …, P. A. Gottlieb. 2004. Bilayer-dependent inhibition of mechanosensitive channels by neuroactive peptide enantiomers. *Nature.* 430:235–240.
85. Harries, W. E., D. Akhavan, …, R. M. Stroud. 2004. The channel architecture of aquaporin 0 at a 2.2-Å resolution. *Proc. Natl. Acad. Sci. USA.* 101:14045–14050.
86. Roux, B., and K. Schulten. 2004. Computational studies of membrane channels. *Structure.* 12:1343–1351.
87. Needham, D., and R. S. Nunn. 1990. Elastic deformation and failure of lipid bilayer membranes containing cholesterol. *Biophys. J.* 58:997–1009.